Mechanism of Charge Transport in DNA: Internally-Linked Anthraquinone Conjugates Support Phonon-Assisted Polaron Hopping

Danith Ly, Laurie Sanii, and Gary B. Schuster*

Contribution from the School of Chemistry and Biochemistry, Georgia Institute of Technology, Atlanta, Georgia 30332

Received May 26, 1999

Abstract: A series of anthraquinone-containing (AQ) DNA conjugates was prepared. In each case, the AQ is linked to the 2′-oxygen of a uridine. Physical and spectroscopic data suggest that the AQ is intercalated in the duplex DNA on the 3′-side of the uracil. Irradiation of the AQ-DNA conjugates with UV light results in piperidine-requiring strand cleavage at GG steps of both the AQ-containing strand and its complement. The AQ-conjugates were designed to have GG steps disposed symmetrically about the AQ intercalation site. The distance dependence of reaction efficiency at GG steps following AQ irradiation was measured by means of an AQ-containing 71 mer having 7 GG steps. The efficiency of reaction in this sequence falls off exponentially with a distance dependence of 0.071 $Å^{-1}$. AQ-containing conjugates were prepared that incorporate 7,8-dihydro-8-oxoguanines (8-OxoG) at various locations. 8-OxoG has a lower oxidation potential than any of the normal DNA bases and serves as a trap for the migrating radical cation. The 8-OxoG is a very effective trap when the radical cation must migrate through it to reach the GG step, it is a less effective trap when it is on the strand complementary to the GG step. These findings support the mechanism for long-range radical cation migration described as phonon-assisted polaron hopping.

Introduction

Electron transfer is one of the simplest and one of the most important reactions in chemistry.[1] Single electron oxidation or reduction often initiates a cascade of reactions resulting in eventual formation of transformed structure. So it is with DNA; a particularly consequential case since these transformed structures may lead to mutations, aging, or disease.[2,3] Electron-transfer reactions occur over short distances, characterized as having atomic or polyatomic dimensions, or on length scales of many Angstroms in polymeric systems. For example, recent efforts have led to a deep understanding of electron (radical anion) and hole (radical cation) transport over long distances in synthetic conducting polymers and in proteins.[4,5]

Although the existence of long-distance charge transport in DNA has been suspected for a long time,[6] and has been demonstrated experimentally,[7−10] its mechanism has been vigorously debated.[11,12] In one view, proteins form an appropriate mechanistic model. Here, compelling experimental and theoretical evidence supports a weakly coupled path through space, peptide backbone, and hydrogen bonds.[13] Translated to DNA, the protein-like model postulates weak electronic coupling through π-electron overlap of the Watson−Crick base pairs. This model predicts a very steep distance dependence for charge-transport with its rate (or efficiency) falling about one decade every 2−3 Å. A second model requires a new paradigm for long-range charge transport in DNA where its well-stacked, duplex structure is characterized as a "π-way" or "molecular wire".[14,15] This model was created to accommodate experiments that seemed to show a distance dependence for charge transport that falls off one decade in 10−20 Å. A clear consequence of charge transport through a molecular wire is the requirement for meaningful electronic coupling between the donor and acceptor through the orbitals of the DNA bridge.[12,16] A third model for charge transport in DNA is based on discrete electron-transfer reactions between neighboring bases or groups of bases.[10,17−20] This "hopping" model operates in synthetic conducting polymers where the observed distance dependence is a ratio of relative rates for hopping and capture of the migrating charge.[4] Charge transport by hopping does not require meaningful electronic coupling between the donor and acceptor over long distances through the DNA bridge. In support of

(1) Mariano, P. S. *Advances in Electron-Transfer Chemistry*; JAI Press: Greenwich, CT, 1991−96; Vol. 1−6.
(2) Demple, B.; Harrison, L. *Annu. Rev. Biochem.* **1994**, *63*, 915−948.
(3) Loft, S.; Poulsen, H. E. *J. Mol. Med.* **1996**, *74*, 297−312.
(4) Emin, D. *Handbook of Conducting Polymers*; Marcel Dekker: New York, 1986; Vol. 2.
(5) Casimiro, D. R.; Richard, J. H.; Winkler, J. R.; Gray, G. B. *J. Phys. Chem.* **1993**, *97*, 13073−13077.
(6) Eley, D. D.; Spivey, D. I. *Trans. Faraday Soc.* **1962**, *58*, 411−415.
(7) Becker, D.; Sevilla, M. D. *Adv. Radiat. Biol.* **1993**, *17*, 121−180.
(8) Gasper, S. M.; Schuster, G. B. *J. Am. Chem. Soc.* **1997**, *119*, 12762−12771.
(9) Nunez, M.; Hall, D. B.; Barton, J. K. *Chem. Biol.* **1999**, *6*, 85−97.
(10) Henderson, P. T.; Jones, D.; Hampikian, G.; Kan, Y.; Schuster, G. B. *Proc. Natl. Acad. Sci. U.S.A.* **1999**, *96*, 8353−8358.
(11) Beratan, D. N.; Priyadarshy, S.; Risser, S. M. *Chem. Biol.* **1997**, *4*, 3−8.
(12) Jortner, J.; Bixon, M.; Langenbacher, T.; Michel-Beyerle, M. E. *Proc. Natl. Acad. Sci. U.S.A.* **1998**, *95*, 12759−12765.
(13) Beratan, D. N.; Onuchic, J. N.; Winkler, J. R.; Gray, H. B. *Science* **1992**, *258*, 1740−1741.
(14) Murphy, C. J.; Arkin, M. R.; Jenkins, Y.; Ghatlia, N. D.; Bossman, S. H.; Turro, N. J.; Barton, J. K. *Science* **1993**, *262*, 1025−1029.
(15) Turro, N. J.; Barton, J. K. *J. Biol. Inorg. Chem.* **1998**, *3*, 201−209.
(16) McConnell, H. M. *J. Chem. Phys.* **1961**, *35*, 508−513.
(17) Meggers, E.; Michel-Beyerle, M. E.; Giese, B. *J. Am Chem. Soc.* **1998**, *120*, 12950−12955.
(18) Ly, D.; Kan, Y.; Armitage, B.; Schuster, G. B. *J. Am. Chem. Soc.* **1996**, *118*, 8747−8748.
(19) Armitage, B. A.; Yu, C.; Devadoss, C.; Schuster, G. B. *J. Am. Chem. Soc.* **1994**, *116*, 9847−9859.
(20) Giese, B.; Wessely, S.; Spormann, M.; Lindemann, U.; Meggers, E.; Michel-Beyerle, M. E. *Angew. Chem., Int. Ed.* **1999**, *38*, 996−998.

10.1021/ja991753s CCC: $18.00
Published on Web 09/24/1999

hopping, recently we and others have reported charge transport through duplex DNA that falls off one decade in ~100 Å.[9,10]

There has been significant progress in the investigation of charge transport in DNA. In an early experiment, Brun and Harriman[21] reported fluorescence quenching of randomly intercalated donors and acceptors and concluded that there is a steep distance dependence for the electron-transfer reaction. In contrast, Barton and Turro reported a series of photophysical and chemical studies using randomly intercalated and covalently linked donors and acceptors. A particularly provocative finding was that the fluorescence of a covalently linked $Rh(phi)_2(phen')_2$ complex is quenched by $Ru(phen')_2(dppz)^{2+}$ ~30 Å away with a rate constant for electron transfer (k_{et}) $\geq 10^{10}$ s^{-1}. This finding, and subsequently reported results, were used to support postulation that DNA behaves like a molecular wire.[14,15] On the other hand, Fukui and Tanaka[22] studied an acridine-containing fluorescer linked internally to DNA by covalent attachment at the phosphate backbone. Their systematic increase of the separation between the fluorescer and the guanine revealed a 10-fold drop over ~1.5 Å. Lewis and co-worker's[23] study of unnatural stilbene-bridged hairpins also indicated a steep dependence. Giese, Michel-Beyerle, and co-workers[17] used a novel chemical reaction to introduce a radical cation in DNA and proposed that it migrates from G to G (intra- and inter-strand) in DNA. A series of recent experiments led Barton and co-workers to the conclusion that DNA duplexes exhibit a wide range of charge-transport efficiencies that appear to be controlled by base stacking and reaction energetics.[9,24−26] These results encouraged their revised proposal that base pair motions control the time scale and degree of coherent charge transport in DNA.

A number of light-activated compounds have been identified that damage DNA by oxidizing its bases as revealed with high sensitivity by monitoring strand cleavage using polyacrylamide gel electrophoresis (PAGE). These compounds include riboflavin,[27,28] naphthalamides,[29] rhodium complexes,[30] and the family of anthraquinone (AQ) derivatives that we have been examining.[18,19,31,32] Despite this broad structural diversity, these compounds have features in common, which point to a shared mode of action. For example, we have shown that irradiation of an intercalated or end-capped AQ leads to selective reaction at the 5′-guanine of GG steps. Comparison of various AQ structures, spectroscopic studies. and the products of these reactions show that this reaction is initiated by rapid electron transfer to the electronically excited AQ from a DNA base to form the quinone radical anion. Reaction of the quinone radical anion with O_2 forms superoxide (O_2^-), regenerates the AQ, and leaves a radical cation ("hole") in the DNA. Examination of DNA duplexes with AQ derivatives covalently linked to their 5′-ends reveals that the hole can be transported to GG steps more than 50 base pairs away.[8,10] In this work, we describe a series of DNA duplexes having AQ derivatives linked to internal positions by covalent attachment to the 2′-carbon atom of a ribose (see Figure 1). Selective irradiation of the AQ with near UV light causes remote damage, revealed as strand cleavage, at GG steps or at strategically placed 7,8-dihydro-8-oxoguanines (8-OxoG). This investigation provides the means to assess the electronic coupling between DNA bases and the ability of a radical cation to hop from one strand to its complement.

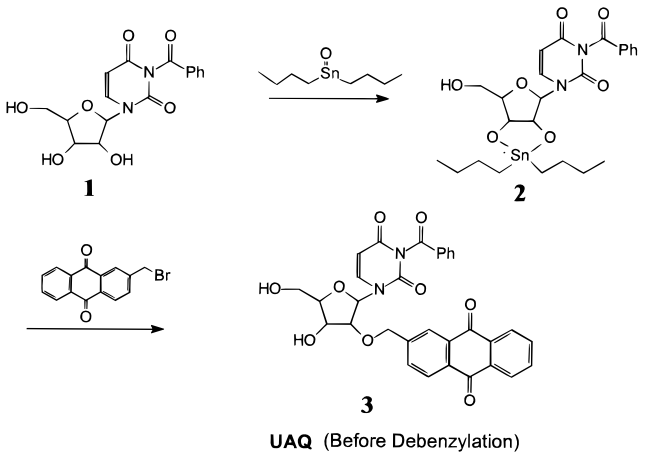

Figure 1. Preparative route for uridine-linked AQ (**UAQ**). This procedure follows the strategy of Broom and co-workers.[39]

Results

(1) Design of AQ-Conjugated DNA Oligonucleotides. Many of the recent experimental systems devised to assess the rate and efficiency of charge transport in DNA incorporate a covalently linked electron acceptor that can be activated chemically or photochemically. In most cases, the acceptor is attached to a terminus of the duplex. In this work we attached the acceptor (an AQ) to the central position of a DNA duplex which has been designed so that it has the same base sequence extending from this central point in both the 5′- and 3′-directions. Pairs of GG steps are located approximately equidistant from the AQ on both the AQ-containing strand and on its complement. This arrangement allows us to modify the charge acceptor in one direction, or one strand, and probe the effect of this modification on transport in the opposite direction or on the complementary strand. The modification we introduce is the substitution of an 8-OxoG for a guanine base in a GG step. Solution and solid-state structural analysis reveals little perturbation to the global structure of B-form DNA from this change.[33,34] However, the oxidation potential of 8-OxoG is ~0.4 V lower than that of guanine,[35] and both experiment and theory agree that this modification provides a deep trap for a migrating radical cation.[36,37] The particular sequence selected for **UAQ-DNA** (Figure 2) is based on our previous finding that leading A-tracts

(21) Brun, A. M.; Harriman, A. *J. Am. Chem. Soc.* **1992**, *114*, 3656−3660.
(22) Fukui, K.; Tanaka, K. *Angew. Chem., Int. Ed.* **1998**, *37*, 158−161.
(23) Lewis, F. D.; Wu, T.; Zhang, Y.; Letsinger, R. L.; Greenfield, S. R.; Wasielewski, M. R. *Science* **1997**, *277*, 673−676.
(24) Kelley, S. O.; Holmlin, E. R.; Stemp, E. D. A.; Barton, J. K. *J. Am. Chem. Soc.* **1997**, *119*, 9861−9870.
(25) Kelley, O. S.; Barton, J. K. *Chem. Biol.* **1998**, *5*, 413−425.
(26) Wan, C.; Fiebig, T.; Kelly, S. O.; Treadway, C. R.; Barton, J. K.; Zewail, A. H. *Proc. Natl. Acad. Sci. U.S.A.* **1999**, *96*, 6014−6019.
(27) Ito, K.; Inoue, S.; Yamamoto, K.; Kawanishi, S. *J. Biol. Chem.* **1993**, *268*, 13221−13227.
(28) Kasai, H.; Yamaizumi, Z.; Berger, M.; Cadet, J. *J. Am. Chem. Soc.* **1992**, *114*, 9692−9694.
(29) Saito, I.; Takayama, M.; Sugiyama, H.; Nakatani, K.; Tsuchida, A.; Yamamoto, M. *J. Am. Chem. Soc.* **1995**, *117*, 6406−6407.
(30) Holmlin, R. E.; Barton, J. K. *Inorg. Chem.* **1995**, *34*, 7−8.
(31) Breslin, D. T.; Coury, J. E.; Anderson, J. R.; McFail-Isom, L.; Kan, Y.; Williams, L. D.; Bottomley, L. A.; Schuster, G. B. *J. Am. Chem. Soc.* **1997**, *119*, 5043−5044.
(32) Henderson, P. T.; Armitage, B.; Schuster, G. B. *Biochemistry* **1998**, *37*, 2991−3000.
(33) Lipscomb, L. A.; Peek, M. E.; Morningstar, M. L.; Verghis, S. M.; Miller, E. M.; Rich, A.; Essigmann, J. M.; Williams, L. D. *Proc. Natl. Acad. Sci. U.S.A.* **1995**, *92*, 719−723.
(34) Oda, Y.; Uesugi, S.; Ikehara, M.; Nishimura, S.; Kawase, Y.; Ishikawa, H.; Inoue, H.; Ohtsuka, E. *Nucleic Acids Res.* **1991**, *19*, 1407−1412.
(35) Sheu, C.; Foote, C. S. *J. Am. Chem. Soc.* **1995**, *117*, 6439−6442.
(36) Prat, F.; Houk, K. N.; Foote, C. S. *J. Am. Chem. Soc.* **1998**, *120*, 845−846.
(37) Saito, I.; Nakamura, T.; Nakatani, K.; Yoshioka, Y.; Yamaguchi, K.; Sugiyama, H. *J. Am. Chem. Soc.* **1998**, *120*, 12686−12687.

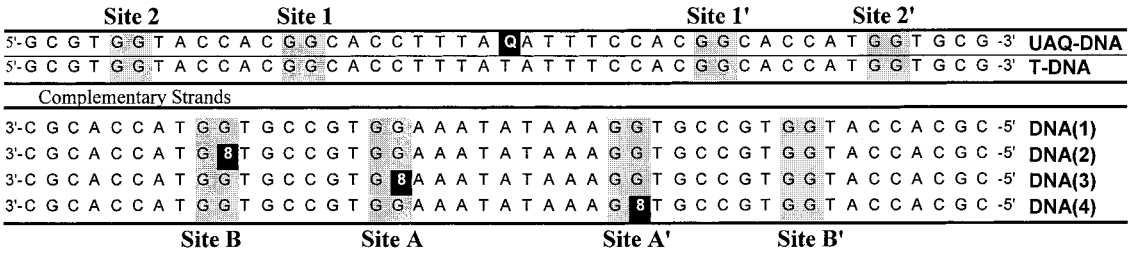

Figure 2. Oligonucleotide sequences: **Q** stands for **UAQ** and **8** stands for 8-OxoG. Strands **DNA(1−4)** are complementary to **UAQ-DNA** and to **T-DNA. UAQ-DNA** and **T-DNA** differ only in that thymidine replaces **UAQ**.

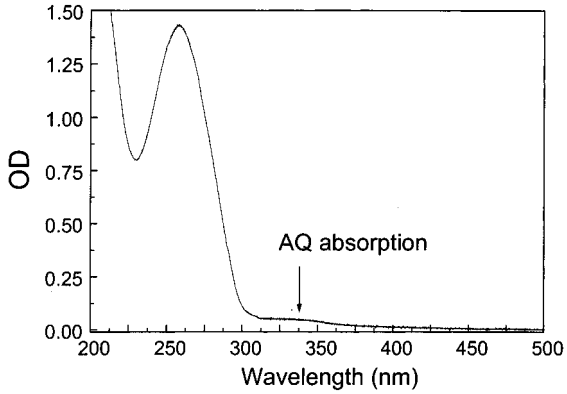

Figure 3. Absorption spectrum of **UAQ-DNA** in phosphate buffer solution at room temperature. The sample was purified by HPLC, which reveals only one peak. The weak absorption band centered at ~330 nm is absent in samples that do not contain a covalently bound AQ.

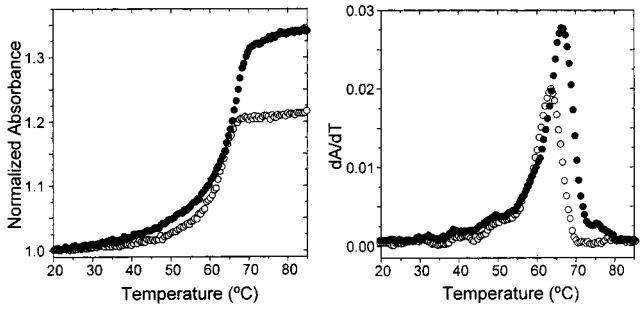

Figure 4. Melting curves for **UAQ-DNA/DNA(1)**, solid circles, and **T-DNA/DNA(1)**, open circles. The melting curves are presented as absolute normalized absorptions, left panel, and as first derivative plots, right panel. The melting behavior was determined in standard phosphate buffer solution containing 2.5 μM of the duplex and monitored at 260 nm.

in the complementary strand give cleavage that is more efficient at GG steps.[18] We prepared centrally linked AQ-DNA conjugates and the series of complementary strands with 8-OxoG modifications. Analysis of their photochemistry permits us to address central questions concerning the mechanism of charge transport in duplex DNA.

(2) Synthesis and Analysis of Internally Linked AQ-DNA and Its Complements. The synthesis of the anthraquinone-containing uridine derivative (**UAQ**, Figure 1) follows the procedure described by Yamana and co-workers.[38]

As its DMT-protected cyanophosphoramide, **UAQ** is readily incorporated into oligonucleotides by simple modification of standard automated, solid-phase DNA synthesis methods. The oligonucleotides we prepared for this work are shown in Figure 2 where **Q** stands for **UAQ,** and **8** stands for 8-OxoG. The synthetic **UAQ-DNA** conjugates were cleaved from their solid support following standard conditions and then purified by HPLC. Their composition and purity were verified by HPLC, mass spectrometry, UV−vis spectroscopy, and PAGE. In particular, matrix assisted laser desorption ionization-time-of-flight mass spectrometry (MALDI-TOF) provides convincing evidence for the composition of the AQ-conjugate. The MALDI-TOF of **UAQ-DNA** yields two sharp peaks with $m/e = 13\,998$ and 7009, corresponding to the singly and doubly charged species, respectively. These values are in excellent agreement with the mass calculated for **UAQ-DNA** of 14 011. Finally, **UAQ-DNA** was 3′-end-labeled with ^{32}P and analyzed by standard sequencing techniques to ensure that it was correctly synthesized. Because of its anthraquinone chromophore, **UAQ-DNA** absorbs at 350 nm (Figure 3) where DNA is normally transparent. This provides a convenient means for monitoring and identifying the AQ-containing conjugate and for the selective optical excitation of the AQ group when it is incorporated in DNA.

(3) Structural Characterization of Duplexes Containing UAQ-DNA. Yamana and co-workers[38] examined the thermal denaturation and circular dichroism (CD) spectroscopy of **UAQ**-containing duplexes. Broom and co-workers[39] applied CD and 2D-NMR spectroscopic techniques as part of a detailed structural analysis of very similar AQ-containing conjugates. Both groups reached similar conclusions: the AQ group is intercalated to the 3′-side of the nucleoside to which it is attached. Broom's findings reveal that the presence of the AQ affects the global structure of the duplex. In particular, at low-temperature multiple conformations of the DNA are detected. However, as the temperature is increased the less stable conformations melt into B-form DNA. This behavior appears to be reproduced in the photochemical results we report below.

We examined the melting behavior of the **UAQ**-conjugated duplexes to assess the binding mode of the quinone. Figure 4 shows the melting curves for duplexes formed between the **T-DNA**, which has the same sequence as **UAQ-DNA** but has a thymine in place of the uridine-bound quinone (see Figure 2), and **UAQ-DNA** with **DNA(1)** which is their complement. These duplexes exhibit cooperative, monophasic melting transitions. The T_m for the AQ-containing duplex is 63.1 °C, which is ~2.3 °C higher than that of the **T-DNA** duplex. No hysteresis is observed for these transitions when sequential heating and cooling experiments are recorded. This demonstrates rapid hybridization kinetics. The melting transition monitored at 330 nm, where only the AQ absorbs, also shows significant hypochromicity. These findings are consistent with those reported by Yamana and by Broom and suggest that the AQ is associated with the duplex by intercalation and stabilized by hydrophobic interaction with adjacent bases.[40]

(38) Yamana, K.; Nishijima, Y.; Ikeda, T.; Gokota, T.; Ozaki, H.; Nakano, H.; Sangen, O.; Shimidzu, T. *Bioconjugate Chem.* **1990**, *1*, 319−324.

(39) Deshmukh, H.; Joglekar, S. P.; Broom, A. D. *Bioconjugate Chem.* **1995**, *6*, 578−586.

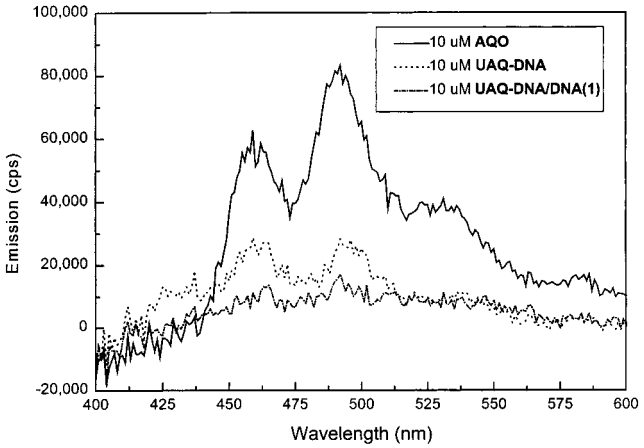

Figure 5. Phosphorescence emission spectra recorded at 77 K in frozen 30% ethylene glycol/sodium phosphate solutions containing 10 μM of **AQO** (a model for the anthraquinone chromophore, see text), solid line; single stranded **UAQ-DNA**, dashed line; or duplex **UAQ-DNA/DNA(1)**, broken line.

Another way of assessing the binding of the AQ in **UAQ-DNA/DNA(1)** is by analysis of phosphorescence quenching. AQ derivatives which have nπ* excited states rapidly intersystem cross to their triplet states[41] and their phosphorescence is readily detected at 77 K. We have shown that the phosphorescence of these quinones is almost completely quenched by electron transfer from an adjacent base when the AQ is intercalated into duplex DNA. In contrast, when the associated quinone is not intercalated, less phosphorescence quenching is observed.[42] Figure 5 shows three phosphorescence spectra recorded in frozen, glassy 30% ethylene glycol/sodium phosphate buffer: 2-(methoxy)methyl-9,10-anthraquinone (**AQO**), which is a model for the quinone chromophore of **UAQ**; **UAQ-DNA** as a single strand, and duplex **UAQ-DNA/DNA(1)**. Internal linkage of the quinone to a single strand of DNA results in ~90% phosphorescence quenching. Significantly, addition of complementary **DNA(1)** results in, essentially, complete quenching. This finding is also consistent with intercalation of the quinone in the **UAQ-DNA/DNA(1)** duplex.

(4) Photochemistry of UAQ-DNA/DNA(1−4). We have reported that irradiation of quinones that are intercalated in duplex DNA, or are covalently linked to a 5′-terminus, leads to long-range damage revealed as strand cleavage at the 5′-guanine of remote GG steps.[10,43] We probed the result of irradiation of internally linked **UAQ-DNA** when it is 5′-labeled with ^{32}P and when its complementary strand, **DNA(1)**, is 5′-labeled. These experiments allow us to assess long-range damage at eight GG steps located in the quinone-containing strand and in its complement. The results obtained depend on the temperature of the irradiated sample.

Figure 6 contains autoradiograms from PAGE experiments following irradiation (λ = 350 nm) of **UAQ-DNA/**(5′-^{32}P)**DNA-(1)** at 20 and at 35 °C in air-saturated phosphate buffer (pH = 7.0). The samples were treated with piperidine to reveal base damage before analysis. Lanes 1, 2, and 6 are controls, which

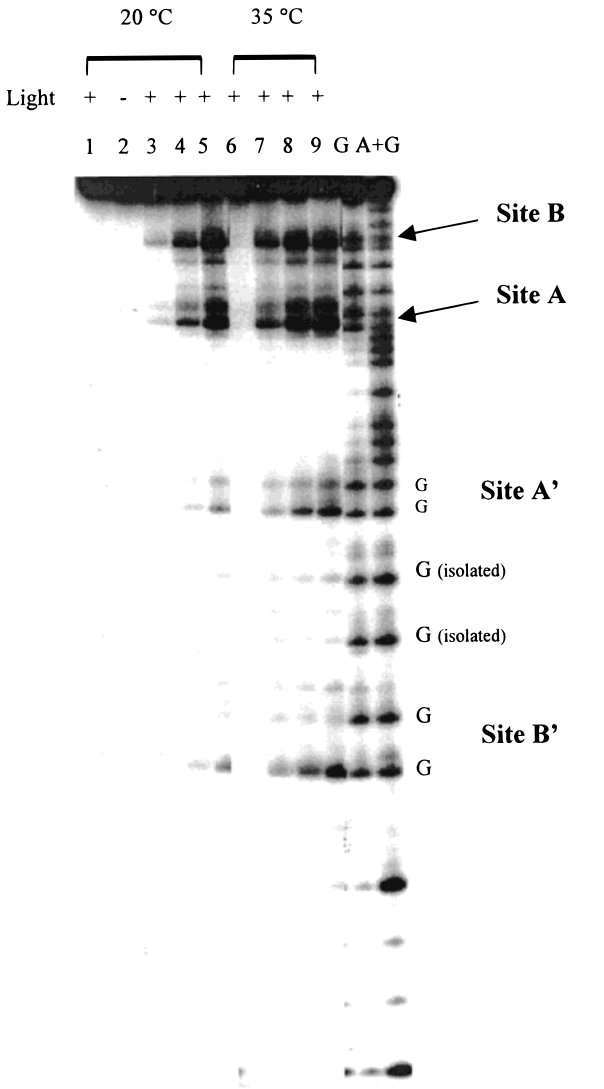

Figure 6. Autoradiogram of a PAGE gel for analysis of strand cleavage from UV irradiation (350 nm) of **UAQ-DNA/DNA(1)** in standard phosphate buffer solution. **DNA(1)** is labeled with ^{32}P at its 5′-terminus. Lanes 1, 2, and 6 are control experiments that show the effect of no irradiation (lane 2) and irradiation for 120 min at 20 °C (lane 1) or at 35 °C (lane 6) but without piperidine treatment. The lanes labeled G and A+G are for Maxam Gilbert sequencing of the DNA. Lanes 3, 4, and 5 (7, 8, and 9) show the results of irradiation for 30, 60, and 120 min, respectively, at 20 °C (35 °C). Identification of the strand cleavage at sites A, A′, B, B′ refers to the designation shown in Figure 2. Identification as "G isolated" locations refers to guanines that are not part of a GG step.

demonstrate that cleavage requires both irradiation and piperidine treatment. Lanes 3, 4, and 5 correspond to 30, 60, and 120 min of irradiation at 20 °C, respectively, and lanes 7, 8, and 9 are for similar irradiation of the sample but carried out at 35 °C. Inspection of Figure 6 shows the expected cleavage at 5′-guanines of remote (from the AQ) GG steps. Interestingly, at 20 °C the GG steps located to the 5′-side of the **UAQ** (sites A and B of Figure 2) are cleaved more efficiently than the corresponding GG steps to the 3′-side of the **UAQ** (sites A′ and B′). This "side-selectivity" depends on the temperature at which the irradiation is carried out and is much reduced at 35 °C. This temperature effect may be related to the phenomenon observed by Broom and by Yamana—conversion of multiple DNA structures to a predominantly standard B-form for **UAQ**-containing duplexes[38,39]—or to changes in the geometry of the

(40) Guckian, K. M.; Schweitzer, B. A.; Ren, R., X.-F.; Sheils, C. J.; Paris, P. L.; Tahmassebi, D. C.; Kool, E. T. *J. Am. Chem. Soc.* **1996**, *118*, 8182−8183.
(41) Loeff, I.; Treinin, A.; Linschitz, H. *J. Phys. Chem.* **1984**, *88*, 4931−4937.
(42) Breslin, D. T.; Schuster, G. B. *J. Am. Chem. Soc.* **1996**, *118*, 8, 2311−2319.
(43) Gasper, S. M.; Armitage, B.; Hu, G. G.; Shui, X.; Yu, C.; Williams, L. D.; Schuster, G. B. *J. Am. Chem. Soc.* **1998**, *120*, 12402−12409.

Figure 7. Sequence for **UAQ-DNA(71)/DNA(5)** a duplex oligonucleotide containing 7 GG steps at various distances (sites 1′, 1−6) from a covalently linked **UAQ** (symbolized by Q in the structure).

anthraquinone at the intercalation site. The photochemical experiments we report below were carried out at 35 °C.

The data in Figure 6 show that reaction at guanines occurs at sites remote from the covalently bound AQ. Damage at a distance such as this may be either intramolecular or intermolecular. We carried out a series of experiments designed to resolve this question. Reaction at guanine is a characteristic of singlet oxygen ($^1O_2$), which might be generated by the triplet state of the AQ. However, $^1O_2$ is known to react with both isolated guanines and with GG steps.[44,45] Inspection of Figure 6 reveals little cleavage at isolated guanines, which suggests that $^1O_2$ is not responsible for a significant fraction of the observed reaction.

We also probed for the involvement of $^1O_2$ by assessing the solvent deuterium isotope effect. It is known that the lifetime of $^1O_2$ increases ∼10-fold when the reaction solvent is changed from H_2O to D_2O, and this change leads to a concomitant increase in reaction efficiency.[46,47] No reactivity increase is observed when this solvent change is made, and this observation, too, rules out a role for $^1O_2$. Additional control experiments show that cleavage at GG steps originates with excitation of the AQ bound to that duplex. Irradiation of an unlabeled, AQ-linked duplex in the presence of a noncomplementary 5′-^{32}P-labeled, GG-containing duplex not having a quinone causes no detectable cleavage of the labeled duplex. These experiments show that the long-distance reaction at GG steps for **UAQ-DNA/DNA(1)** must be intramolecular.

The results shown in Figure 6 also indicate that the cleavage efficiency depends on the distance between the 5′-G and the AQ. The proximal GG steps (sites A and A′) of **DNA(1)** are cleaved more efficiently than are the distal steps (sites B and B′). However, it is difficult to reach quantitative conclusions about the distance dependence from this experiment because there are only two distances to compare. Figure 7 shows the structure of a duplex 71-mer. One strand, **UAQ-DNA(71)**, has a UAQ linked in a position that is identical with that of **UAQ-DNA** and has been extended in the 5′-direction so that its complement, **DNA(5)**, includes a total of six GG steps on the 3′-side of the AQ. Irradiation of **UAQ-DNA(71)/(5′-^{32}P)DNA-(5)** and subsequent treatment with piperidine, as described above, gives the PAGE autoradiogram shown in Figure 8. The cleavage efficiency clearly falls off with the distance between the AQ and the 5′-G of the GG step. Remarkably, cleavage is observed at GG_6, which is ∼160 Å from the AQ intercalation site.

The distance dependence for radical cation migration in **UAQ-DNA(71)/(5′-^{32}P)DNA(5)** was determined by quantification of the cleavage efficiency. The reaction efficiency at each GG step was determined by measuring the total β-radiation in the 3′- and 5′-G bands, subtracting the corresponding background radiation for each band (Figure 8, lane 2), and normalizing the data so that site 1 ≡ 1.0. The results are shown graphically in Figure 9, which is a semilog plot of reaction efficiency against distance. The slope of this line determined from three independent experiments is -0.017 ± 0.004 Å^{-1} which corresponds to a fall off in cleavage efficiency of one decade over ∼135 Å. Related experiments with transition metal-linked DNA derivatives show a similar very shallow distance dependence.[9]

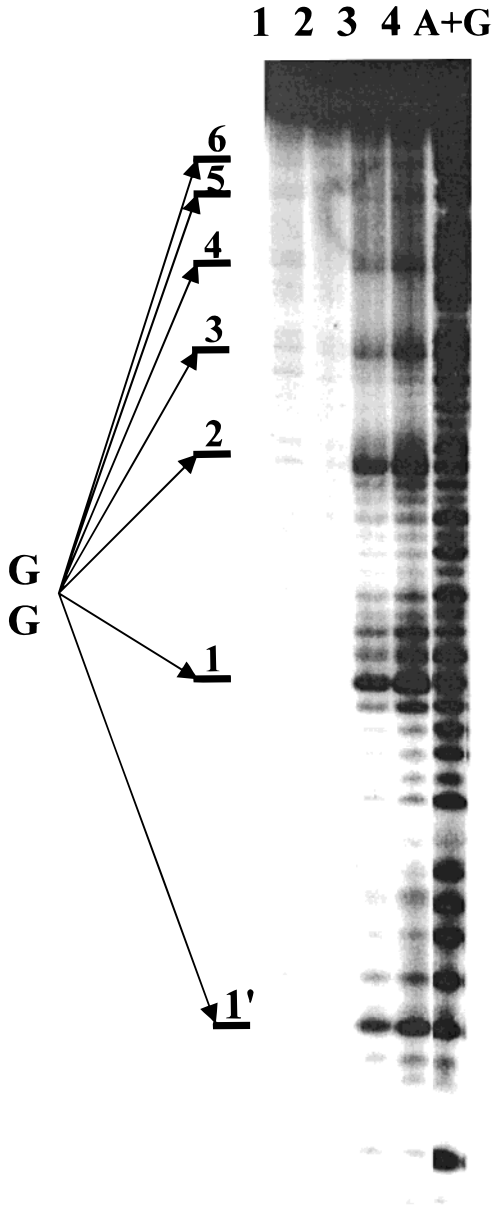

Figure 8. Autoradiogram of a PAGE gel for analysis of strand cleavage from UV irradiation (350 nm) of **UAQ-DNA(71)/DNA(5)** in standard phosphate buffer solution at 35 °C. **DNA(5)** is labeled with ^{32}P at its 5′-terminus. Lanes 1 and 2 are control experiments that show the results of irradiation with no piperidine treatment and piperidine treatment with no irradiation, respectively. Lanes 3 and 4 show the result of 60 and 120 min, respectively, of irradiation followed by piperidine treatment. The lane labeled A+G is for Maxam Gilbert sequencing of the DNA.

Figure 10 shows results from irradiation of **UAQ/(5′-^{32}P)-DNA(1−4)** presented schematically.[48] The arrows in this figure point to the major cleavage sites and their lengths represent the relative amount of cleavage as determined by densitometry of

(44) Blazek, E. R.; Peak, J. G.; Peak, M. J. *Photochem. Photobiol.* **1989**, *49*, 607−613.
(45) Floyd, R. A.; West, M. S.; Eneff, K. L.; Schneider, J. E. *Arch. Biochem. Biophys.* **1989**, *273*, 106−111.
(46) Rogers, M. A. J.; Snowden, P. T. *J. Am. Chem. Soc.* **1982**, *104*, 5541−5543.
(47) Showen, K. B.; Showen, R. L. *Solvent Isotope Effects on Enzyme Systems*; Academic Press: New York, 1982; Vol. 87.

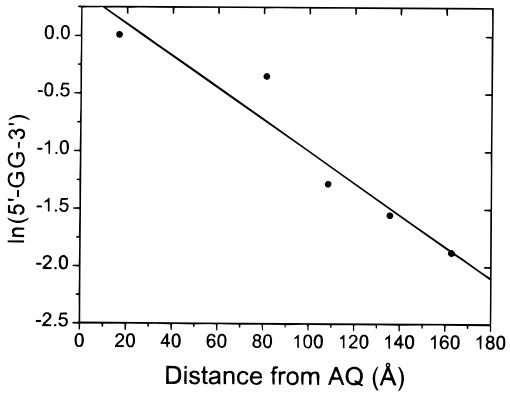

Figure 9. A semilog plot of cleavage efficiency determined by integrating the total counts in the bands for both the 3′- and 5′-G from the PAGE gel shown in Figure 8 with a β counter at sites 1−6 versus the distance in Å between the 5′-G and the AQ assuming an average distance of 3.4 Å per base pair. The line is a least-squares fit to the cleavage intensity data.

the autoradiograms. The sequence of **DNA(2)** is identical to **DNA(1)** except that 8-OxoG has been substituted for the 5′-G of the distal GG step on one side of the **UAQ** (site B). As expected[8] cleavage at the 8-OxoG and its adjacent guanine is enhanced when compared with cleavage in **DNA(1)**, Figure 10B. Significantly, this substitution has no measurable effect on cleavage at the proximal GG step at site A or on either the proximal or distal GG steps to the other side of the UAQ (sites A′ and B′). This result becomes more meaningful when compared with related findings from irradiation of **UAQ-DNA/(5′-^{32}P)DNA(3)**. In this case an 8-OxoG replaces the 5′-G of the proximal GG step at site A, Figure 10C. Cleavage at the distal GG step on the same side, site B, is reduced, but there is no measurable effect on the cleavage of either the proximal or distal GG steps located on the other side of the **UAQ** (sites A′ and B′). Finally, analysis of the irradiation of **UAQ-DNA/(5′-^{32}P)DNA(4)**, where an 8-OxoG is substituted for the 5′-G at the proximal GG step on the other side of the **UAQ** (site A′, Figure 10D), results in reduced cleavage at the distal GG on that side (site B′) with no effect on cleavage on the opposite side of the AQ, (sites A and B). These results substantiate those from **UAQ-DNA/(5′-^{32}P)DNA(3)**. These findings confirm that 8-OxoG is a trap for radical cations migrating on the DNA strand containing the 8-OxoG. Further, reaction at a GG step positioned between an 8-OxoG and the intercalated quinone is hardly affected by the 8-OxoG. Finally, substitution of an 8-OxoG does not effect the migration of a radical cation to GG steps on the opposite side of the intercalated AQ.

Figure 11 shows the results of experiments with **(5′-^{32}P)-UAQ/DNA(1−4)** that permit analysis of the effect of irradiation on the DNA strand that contains the covalently linked AQ. In each case, GG-selective cleavage at proximal (sites 1 and 1′, Figure 2) and distal (sites 2 and 2′) positions is observed. Interestingly, substitution of an 8-OxoG for the 5′-G on the complementary strand between the proximal and distal GG steps of the AQ-containing strand, **(5′-^{32}P)UAQ/DNA(2)**, reduces cleavage at the distal step (site 2) but not at the proximal one (site 1, Figure 11B). This finding shows that an 8-OxoG functions only as a weak trap for radical cations migrating on a complementary strand. Significantly, this experiment, and the others with **(5′-^{32}P)UAQ/DNA(3)** and **(5′-^{32}P)UAQ/DNA(4)** shown in Figure 11C and 11D, reveal that incorporation of an 8-OxoG on one side of the DNA duplex has little effect on cleavage at the GG steps that occurs on the opposite side of the AQ.

(48) The autoradiograms for **UAQ-DNA** with **DNA(1−4)** labeled at its 5′-end and with **UAQ-DNA** labeled at the 3′-end with ^{32}P are included as Supporting Information to this paper.

Discussion

The experiments reported here were designed primarily to answer a simply stated question: Does a radical cation migrating in duplex DNA "know" of a trap before the trap is encountered? This question has relevance to the debate over the mechanism and distance dependence of radical cation migration. Two cases can be considered as limiting extremes. If DNA is a molecular wire, the radical cation is essentially instantaneously delocalized through a continuous molecular orbital of a well-stacked, B-form helix.[12,24] In this orbital, each base pair is in electronic contact with every other, and once a charge is injected into the π-electron stack, it is delocalized throughout this entire orbital. In this model, the radical cation can travel almost instantaneously through the DNA independent of base sequence and distance.[15] If this is the operative mechanism, a radical cation injected in the duplex would be in electronic contact with a remote trap, and that contact will influence the direction of radical cation migration. On the other hand, the hole-hopping model presumes discrete molecular orbitals at each base with no significant electronic overlap between adjacent base pairs.[17,18] One-electron oxidation generates a localized radical cation that migrates (hops) by an activated process requiring local structural distortion of the DNA. According to this model, the rate of migration will be temperature- and sequence-dependent, and an unconnected trap will not influence migration direction through bases that precede the trap in the sequence. The results of our experiments, and those recently reported by others, reveal a complex reality containing features from both of these limiting models.[9,26]

(1) Trapping the Radical Cation with 8-OxoG. We consider the ideal trap for a migrating radical cation to be a modified base that does not distort the structure of the DNA duplex and has an oxidation potential (E_{ox}) significantly below that of any of the normal DNA bases.[33,34] 8-OxoG was selected for use as the trap on this basis. This modified base is often detected as a product of DNA oxidation and, consequently, it has been extensively studied.

We expected that 8-OxoG would be an effective trap for a migrating radical cation based on its E_{ox}. Foote and Sheu report that E_{ox} of 8-OxoG is 0.4−0.5 V below that of guanine, the most easily oxidized normal base (both determined as their *tert*-butyldimethylsily protected nucleoside derivatives).[35] The difference in E_{ox} between guanine and adenine (the next most easily oxidized normal DNA base, see below) is 0.13 V.[49] Consequently by hole hopping, the migration of a radical cation localized on an 8-OxoG to any other base will have a much greater activation energy than for any other migration step. This step will be slower, and irreversible reactions that consume the radical cation will be more efficient at this site than at others. In this sense, the radical cation will be trapped at the 8-OxoG by irreversible reaction. Alternatively, if the π-electrons of well-stacked base pairs form a continuous orbital, then the lower E_{ox} for 8-OxoG requires a higher radical cation density at this site and, consequently, the irreversible reactions that consume the radical cation will be more likely there. Thus, enhanced reactivity at 8-OxoG, which has been verified experimentally[8] and explained theoretically,[36] cannot distinguish between the

(49) Steenken, S.; Jovanovic, S. V. *J. Am. Chem. Soc.* **1997**, *119*, 617−618.

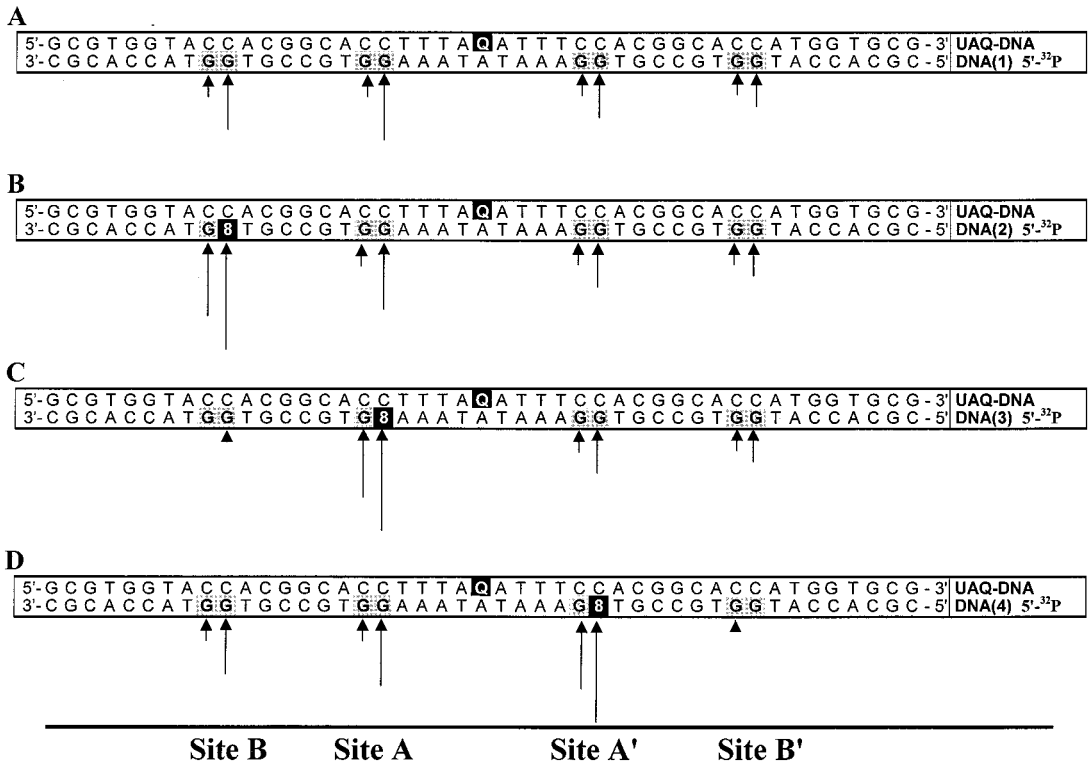

Figure 10. Schematic representation of cleavage efficiencies for irradiation (350 nm, 35 °C) of **UAQ-DNA** as duplexes with **DNA(1−4)** which has been labeled with ^{32}P at the 5′-end. Q stands for UAQ, and 8 stands for substitution of a guanine by an 8-OxoG. The efficiency of cleavage at each GG (or G**8**) for sites A,A′,B,B′ was assessed by determination of the density of the autoradiogram[48] at that site and subtracting the measured density at that site from its "dark control" (an identical sample that was not irradiated) Both the dark controls and "light controls" (irradiated samples not having a linked to AQ group) show some background cleavage at the G**8** sites, but this is well below the amount of irradiation-induced cleavage at these sites. The arrow lengths indicate the relative amounts of cleavage.

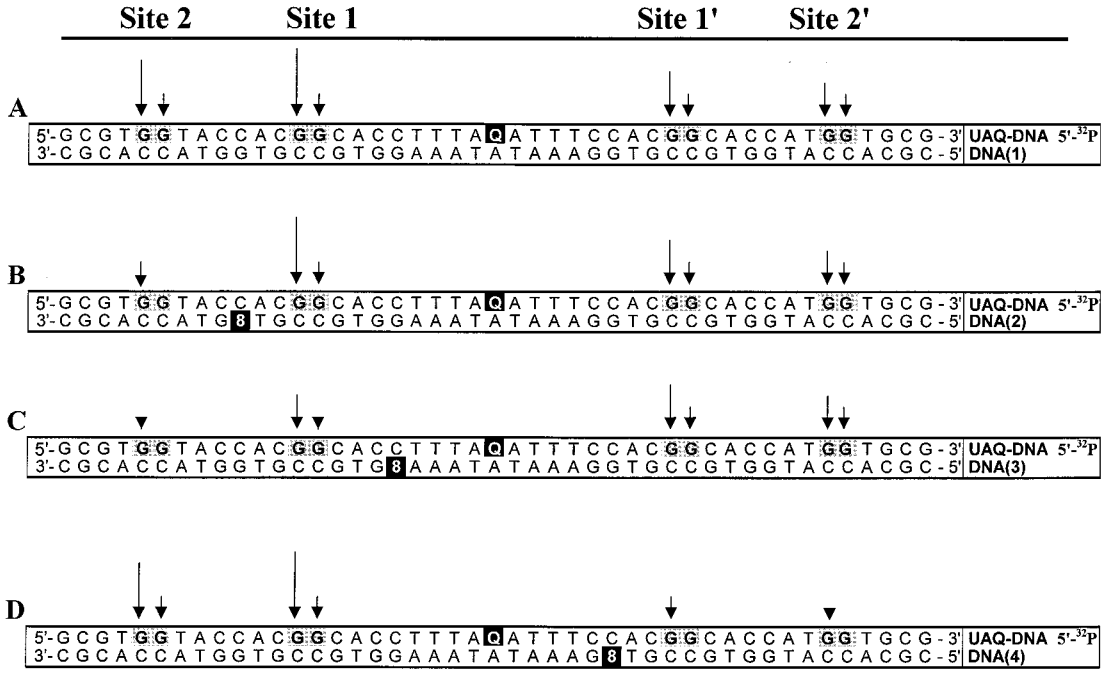

Figure 11. Schematic representation of cleavage efficiencies for irradiation (350 nm, 35 °C) of **UAQ-DNA**, which has been labeled with ^{32}P at the 3′-end, as duplexes with **DNA(1−4)**. Q stands for UAQ, and 8 stands for substitution of a guanine by an 8-OxoG. The efficiency of cleavage at each GG was assessed by determination of the density of the autoradiogram[48] at that site and subtracting the measured density at that site from its "dark control" (an identical sample that was not irradiated). The arrow lengths indicate the relative amount of cleavage at each GG for site 1,1′,2,2′.

limiting mechanistic extremes. However, the systems reported here provide similar paths for migration toward or away from an 8-OxoG trap. These experiments do permit differentiation of these choices.

(2) Structural and Electronic Model for UAQ-DNA. Our work and that of Yamana[38] and Broom[39] leads us to accept the model for the structure of the covalently linked **UAQ** presented in Figure 12. In this model, the AQ is intercalated in the site

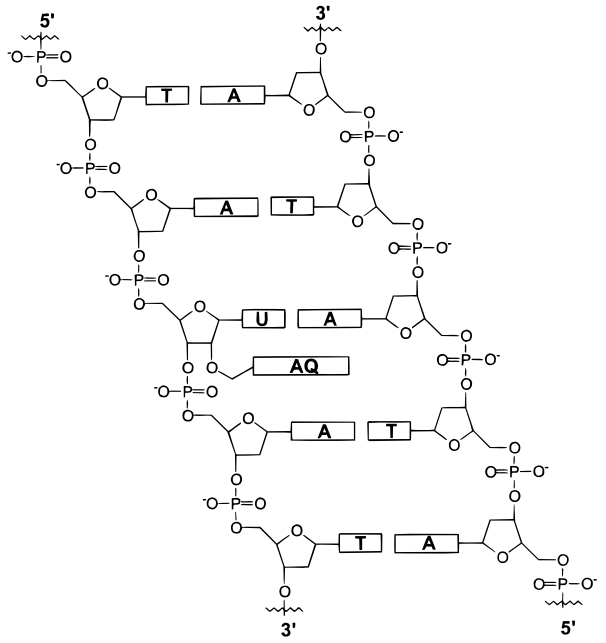

Figure 12. Assumed structure of UAQ intercalated in duplex DNA based upon the NMR spectroscopic data of Broom and co-workers[39] and the melting data and spectroscopic evidence described in the text.

Table 1. Calculated Free Energy Changes for One-Electron Oxidation of DNA Bases by Triplet AQ

	guanosine	adenosine	cytidine	thymidine
E (V)	1.29[a]	1.42[a]	1.6	1.7
ΔG_{ET} (eV)[b]	−0.89	−0.76	−0.58	−0.48

[a] Oxidation potentials for DNA nucleosides from Steenken and Jonanovic.[49] [b] AQ triplet energy (E_T = 2.76 eV)[19] and reduction potential (−0.58 V vs SCE).[42] The free energy changes for one-electron transfer from a particular base to AQ*[3] were calculated with the Rehm−Weller equation.[50]

on the 3′-side of its attached uridine. A significant characteristic of this model is that the long axis of the anthraquinone is parallel to the long axis of the base pairs at the intercalation site. This orientation is consistent with that determined by X-ray crystallography for a related anthraquinone derivative.[43] The bases that form this intercalation site are an A and a T on the complementary strand and the U and an A on the quinone-containing strand. As can be seen from the data in Table 1, which were calculated from the E_{ox} of the DNA bases and the Rehm−Weller equation,[50] oxidation of these bases by the excited singlet or triplet state of the AQ is exothermic. An important implication of this structure and that thermodynamic fact is that the AQ is capable of oxidizing any of the bases that surround it. This suggests that a radical cation can be injected in either the 3′- or 5′-direction on the quinone-containing strand and in its complementary strand.

Time-resolved laser spectroscopy experiments with noncovalently linked quinones reveal that the initial electron transfer from a base to form the AQ radical anion occurs in less than 20 ps.[19] Spectroscopic and chemical experiments show that the unlinked quinone radical anion is quenched by O_2 to form superoxide thus regenerating the AQ and leaving a base radical cation with no partner for annihilation. Consequently, the rate of quenching by O_2, in part, sets the time scale for migration and subsequent reactions of the radical cation. A radical cation generated on the 3′- or 5′-side of the **UAQ** cannot cross to the opposite side because the AQ is a barrier and especially because re-encounters with the quinone radical anion will cause its consumption. This requirement allows us to distinguish hole hopping from radical cation transport through a continuous orbital formed from overlapped DNA bases.

(3) Side-Selection of Radical Cation Migration. The effect of temperature, shown in Figure 6, on the side selection for cleavage at the 5′-G of GG steps was unexpected. At 20 °C, more strand cleavage occurs to the 5′-side of the **UAQ** strand, even though the GG steps on the 3′-side are closer to the quinone than are those on the 5′-side. This side selection may be due to a structural distortion caused by the covalently linked quinone since NMR spectroscopy reveals a transformation to standard B-form DNA at this temperature. This view is supported by a recent NMR spectral study of DNA with intercalated ligands, which shows propagation of structural perturbation.[51] However, there is more than this in the temperature-dependent behavior to consider. The temperature effect may also be due to a change in the intercalation geometry of the anthraquinone or to a structure-dependent change in the hole-trapping rate. Since the overall cleavage efficiency comes from a ratio of rates, it is not possible with the available data to distinguish these possibilities. Because of this uncertainty, we carried out all experiments at 35 °C where the structure seems to be well defined.

(4) Intra-Strand DNA Cleavage Induced by an Internally-Linked AQ. The results displayed in Figure 10 are a rich source of information about the mechanism of hole migration in duplex DNA. Figure 10A shows that irradiation of **UAQ-DNA/DNA-(1)** at 35 °C leads to damage on the **DNA(1)** strand at GG steps located both on the 5′- and 3′-side of the AQ with similar efficiency. This experiment reveals, too, that the cleavage efficiency drops off with distance from the AQ. Cleavage at the distal GG steps (sites B and B′) is less efficient than the cleavage at the proximal positions (sites A and A′). The distance dependence of cleavage efficiency is discussed more fully below. Figure 10C shows the effect of substituting an 8-OxoG for a proximal G located at site A. There are two consequential findings from this experiment. First, cleavage at the distal GG step on that side of the quinone (site B) is greatly reduced. Second, neither the proximal nor the distal GG step on the other side of the AQ (sites A′ and B′) are affected by this substitution. Compare this result to that shown in Figure 10B where the 8-OxoG is substituted for a G in the distal GG step at site B. Here, there is little effect on GG cleavage either at the proximal GG (site A) or at the two GG steps on the other side of the AQ (sites A′ and B′). These findings show that 8-OxoG is an efficient trap when the migrating radical cation must pass through it.

Absorption of light by the AQ forms its excited state. The next step in the postulated mechanism is one-electron oxidation of a base at the intercalation site by this excited state. If the π-electrons of the DNA bases were overlapped to form a continuous orbital, then substitution of 8-OxoG to the 3′-side of the AQ, as in **DNA(2)** and in **DNA(3)**, should favor migration to that side. It does not. The data in Figure 10B and C show that the cleavage efficiency on the side opposite the 8-OxoG is unaffected by this substitution. Consequently, we conclude that the excited AQ is not in electronic contact with the 8-OxoG when the migration selection is determined. This result is consistent with the hole hopping mechanism for radical cation migration but not with the characterization of DNA as a molecular wire.

(5) Strand-to-Complementary-Strand Radical Cation Migration. The experiments shown in Figure 11 address issues

(50) Rehm, D.; Weller, A. *Isr. J. Chem.* **1970**, *8*, 259.

(51) Spielmann, H. P. *Biochemistry* **1998**, *37*, 16863−16876.

associated with radical cation migration in the AQ-containing strand. In particular, these results allow us to assess the effect of an 8-OxoG trap on a radical cation that appears to migrate to the complementary strand. This is particularly relevant because Giese and co-workers recently postulated a mechanism for radical cation transport in DNA that requires cross-strand G-to-G migration.[17,20] Others reports indicate that charge can migrate from strand-to-strand through hydrogen bonds.[52,53]

Figure 11A shows that irradiation of (**5′-^{32}P)UAQ-DNA/DNA(1)** at 35 °C leads to piperidine-requiring strand cleavage at the 5′-guainines of all four GG steps on **UAQ-DNA**. The GG steps to the 5′-side of the AQ (sites 1 and 2) are cleaved with somewhat greater efficiency than those on the 3′-side (sites 1′ and 2′), and the proximal steps (sites 1 and 1′) are cleaved with slightly greater efficiency than the distal GG steps (sites 2 and 2′). These results mirror the findings shown in Figure 10A (where the complementary strand is labeled) and show that migrating radical cations cause reactions on both strands of the duplex.

Parts B, C, and D of Figure 11 show the results of placing an 8-OxoG at various locations on the strand complementary to (**5′-^{32}P)UAQ-DNA**. In each case, there is no significant effect on cleavage efficiency for GG steps located on the opposite side of the AQ from the 8-OxoG. This finding parallels those discussed above and supports the conclusion that normal B-form DNA does not form a continuously overlapped π-orbital. Further, if the 8-OxoG is placed after a GG step in the complementary strand, as it is for the proximal site shown in Figure 11B, there is no reduction of cleavage at that site. This finding, too, supports the previous discussion and conclusion that 8-OxoG acts as an efficient trap only when the migrating radical cation must pass through it. Finally, if the 8-OxoG is before a GG step in the complementary strand, as it is in the experiments shown in parts B, C, and D of Figure 11, then radical cation migration to the distant GG step is inhibited somewhat, but it is not stopped. This is most clearly shown in Figure 11C where an 8-OxoG on the complementary strand results in less than complete reduction in cleavage efficiency at the proximal and distal GG steps (sites 1 and 2) of the **UAQ-DNA** strand. Evidently, radical cations migrating in the strand containing an 8-OxoG are trapped more effectively than radical cations migrating in the complementary strand. This finding shows that strand-to-strand hopping is less efficient than migration along a strand for the sequence examined.

(6) Distance Dependence of Radical Cation Migration. The results shown in Figure 9 demonstrate a very shallow distance dependence for radical cation migration in **UAQ-DNA(71)/(5′-^{32}P)DNA(5).** This result parallel our findings for a series of AQ-DNA conjugates with the quinone linked covalently to a 5′-end[10] and for metal-linked systems recently reported by Barton and co-workers.[9] The approximately linear relationship that is revealed in Figure 9 and the fall-off in cleavage efficiency of one decade over 130 Å require careful consideration of the mechanism for hole migration. Neither the superexchange nor the hole-hopping models can easily accommodate these results.

We have avoided using the symbol β to characterize the distance dependence for radical cation migration. The origin and common usage of this symbol implies a specific mechanism of reaction, particularly, migration by superexchange through bridge orbitals.[16] A compelling argument against operation of this mechanism is that these experiments require β to be ~0.017 Å^{-1}. This is a value far too small to be accommodated by the superexchange mechanism.[54] We have proposed phonon-assisted polaron hopping as a mechanism for radical cation migration in duplex DNA. In this case the magnitude of the slope in Figure 9 (γ) is not a measure of superexchange, but it is determined by a ratio of rate constants for radical cation hopping and reaction.[10]

(7) The Mechanism of Radical Cation Transport in Duplex DNA. Two extreme models were considered in presenting and discussing the results of our experiments. These models can be characterized as zero-delocalization (hole-hopping) and as infinite delocalization (molecular wire). In a recent report, Jortner analyzed charge transport in DNA[12] in terms of these two models (termed sequential hole transport and superexchange) and identified the interesting circumstance where both operate in parallel.[12] The data reported here are consistent with hole hopping and not with infinite delocalization. However, the results argue against such a strict mechanistic differentiation. In particular, a potential flaw in the strict hole-hopping model is that it fails to consider that the structure of DNA is dynamic on the time scale of hole migration. Recent experiments indicate a liquidlike internal structure for DNA where small amplitude motions occur on short time scales.[55] Dynamic NMR experiments show that sugar and base motions occurs on time scales of 30−300 ps.[56−58] We have suggested that dynamical structural variation of DNA "mixes" the hole-hopping and continuous orbital mechanisms for radical cation transport. This concept is part of the phonon-assisted polaron like hopping mechanism.[10]

The key concept in the polaron-like hopping model is that injection of charge into DNA distorts its structure. It is expected that the structure of DNA will respond rapidly to the introduction of a base radical cation. One likely structural change is a reduction of the intra-base pair distance. A second is a change in the unwinding of the DNA. Unwinding will increase the π-electron overlap and stabilize the radical cation.[59] A third possible structural change is a shift in proton position of the hydrogen bonds that form the Watson−Crick base pairs.[60,61] It is the total of these and other possible distortions that we described as a polaron-like species—a self-trapped local distortion of the DNA structure with increased electronic overlap between bases. In this model, the radical cation is delocalized within the few base pairs of the polaron, and its transport therein may appear to be instantaneous. The results described above indicate that the polaron, for the particular base sequences we investigated, does not extend from the AQ as far as the closest 8-OxoG—a distance of five base pairs. If it did, the inclusion of an 8-OxoG would dictate side-selection, and it does not.

Consideration of the internal structural dynamics of DNA led to the suggestion that the polaron migrates by hopping. By this, we mean that migration of the polaron occurs in discrete steps. A hopping step occurs when some number of base pairs leave and join the polaron because of internal motion (structural

(52) Osuka, A.; Nakajima, S.; Okada, T.; Taniguchi, S.; Nozaki, K.; Ohno, T.; Yamazaki, I.; Nishimura, Y.; Mataga, N. *Angew. Chem., Int. Ed. Engl.* **1996**, *35*, 92−95.

(53) Hayashi, T.; Miyahara, T.; Kumazaki, S.; Ogoshi, H.; Yoshihara, K. *Angew. Chem., Int. Ed. Engl.* **1996**, *35*, 1964−1966.

(54) Priyadarshy, S.; Risser, S. M.; Beratan, D. N. *J. Phys. Chem.* **1996**, *100*, 17678−17682.

(55) Brauns, E. B.; Murphy, C. J.; Berg, M. A. *J. Am. Chem. Soc.* **1998**, *120*, 2449−2456.

(56) Borer, P. N.; Pante, S. R.; Kumar, A.; Zanatta, N.; Martin, A.; Hakkinen, A.; Levy, G. C. *Biochemistry* **1994**, *33*, 2441−2450.

(57) Kojima, C.; Ono, A.; Kainosho, M.; James, T. L. *J. Magn. Reson.* **1998**, *135*, 1333−1337.

(58) Georghiou, S.; Bradrick, T. D.; Philippetis, A.; Beechem, J. M. *Biopys. J.* **1996**, *70*, 1909−1922.

(59) Sriram, M.; Wang, A. H.-J. *Structure of DNA and RNA*; Hecht, S. M., Ed.; Oxford University Press: New York, 1996; pp 105−143.

(60) Steenken, S. *Biol. Chem.* **1997**, *378*, 1293−1297.

(61) Steenken, S. *Free Rad. Res. Commun.* **1992**, *16*, 349−379.

reorganization). These internal motions might be some combination of changes in winding or inclination angle and shifts in the location of protons involved in hydrogen bonding. We refer to these motions collectively as phonons. Thus, this mechanism for radical cation migration is termed phonon-assisted polaron hopping.

In principle, the rate of polaron hopping must depend on the local base sequence. Examination of Figures 7 and 9 show that for **UAQDNA(71)/DNA(5)**, there is no conspicuous sequence dependence in the case examined. There is no regularity in the sequence between the five GG steps of this compound, but the distance dependence revealed in Figure 9 appears to be essentially constant. We have suggested that this apparent insensitivity of the hopping rate is a consequence of sequence averaging. Structural distortion of the DNA around the radical cation delocalizes the electron deficiency over several base pairs. Evidence in support of this proposal is found in Saito's calculation of sequence-dependent ionization potentials for guanines.[37] Similarly, polaron-hopping steps of varying length average differences that would be encountered if the radical cation hopped exclusively from base to base. This model does not require that averaging eliminate all differences between DNA sequences.

The experiments described above incorporating 8-OxoG in the DNA sequence reveal a limit to how much averaging of DNA structure in the polaron model is possible. A polaron in which an 8-OxoG replaces a G will has a significantly reduced free energy. Evidently, this stabilization of the polaron reduces the rate of its hopping and increases the probability that the radical cation will be irreversibly trapped at this site.

Experimental Section

General. ^{1}H and ^{13}C NMR spectra were recorded on a Varian 300 MHz spectrometer. ^{31}P NMR were recorded on a Bruker 400 MHz spectrometer. Radioactive isotopes [γ-^{32}ATP] and [α-^{32}ddATP] were purchased from Amersham Bioscience. T4 polynucleotide kinase and terminal deoxynucleotidyl transferase (TdT) were purchased from Pharmacia Biotech and stored at −20 °C. 8-OxoG-modified and unmodified oligonucleotides (gel filtration grade) were obtained from the Midland Certified Reagent Company. Internally linked anthraquinone oligonucleotides were synthesized on an Applied Biosystems DNA synthesizer and were purified by reverse-phase HPLC. The extinction coefficients of the unmodified oligonucleotide were calculated using the nearest-neighbor values, and the absorbance was measured at 260 nm. Anthraquinone-modified oligonucleotide solution concentrations were determined the same way as that of the unmodified oligomers except that an anthraquinone was replaced with adenine in the extinction coefficient determination. Ion-exchange and reverse-phase HPLC were performed on a Hitachi system using a Vydac column. Matrix assisted laser desorption ionization time-of-flight (MALDI-TOF) mass spectrometry of the conjugate strands was performed at the Midland Certified Reagent Company. The buffer solution used in all DNA experiments was 10 mM sodium phosphate at pH = 7.0. UV melting and cooling curves were recorded on a Cary 1E spectrophotometer equipped with a multicell block, temperature controller, and sample transport accessory. Phosphorescence emission spectra were measured on a Spec Fluorolog spectrofluorimeter.

***N*^{3}-Benzoyluridine (1).** Uridine (2.44 g, 10.0 mmol) was added to a 100 mL round-bottom flask containing pyridine (40 mL, 495 mmol) and stirred at room temperature until the uridine was completely dissolved. To this solution, chlorotrimethylsilane (6.4 mL, 50.4 mmol) was added while stirring (a white precipitate formed upon addition). The mixture was stirred for 20 min after the addition was completed. Benzoyl chloride (5.8 g, 41.3 mmol) was then added slowly, and the mixture was stirred for 2 h, cooled in an ice bath, and then extracted twice with ethyl acetate (2 × 200 mL). The organic fractions were combined, washed with brine, and dried over Na_2SO_4. Purification by flash column chromatography (silica gel, CH_2Cl_2/MeOH = 7:1, R_f = 0.3). Yield 3.30 g (95%). ^{1}H NMR (DMSO-d_6) δ 3.55−3.70 (m, 2H, $H_{2'}$ and $H_{3'}$), 3.75 (q, 1H, $H_{4'}$), 4.00−4.12 (m, 2H, $H_{5'}$), 5.10 (d, 1H, $C_{2'}$-OH), 5.18 (t, 1H, $C_{5'}$-OH), 5.50 (d, 1H, $C_{3'}$-OH), 5.77 (d, 1H, H_1), 5.95 (d, 1H, uracil H_5), 7.63, 7.78 and 7.97 (m, 7H, AQ), 8.18 (d, 1H, uracil H_6).

2′,3′-*O*-(Dibutylstannylene)-*N*^{3}-benzoyluridine (2). *N*^{3}-Benzoyluridine (**1**, 2.80 g, 8.1 mmol) and dibutyltin oxide (2.03 g, 8.2 mmol) were heated at reflux in anhydrous methanol (400 mL) for 2 h. When the solution turned clear, the solvent was removed under reduced pressure and the residue was dried under vacuum to give the desired crude product in ∼95% purity. ^{1}H NMR (DMSO-d_6) δ 0.80−1.60 (m, 18H, alkyl chain), 3.45−3.80 (m, 3H, $H_{2'}$, $H_{3'}$ and $H_{4'}$), 4.10−4.20 (m, 2H, $H_{5'}$), 5.10 (t, 1H, $C_{5'}$-OH), 5.60 (d, 1H, $H_{1'}$), 5.95 (d, 1H, uracil H_5), 7.50−8.00 (m, 7H, AQ), 8.12 (d, 1H, uracil H_6).

BzU(2′-UAQ) (3). 2′,3′-*O*-(Dibutylstannylene)-*N*^{3}-benzoyluridine (**2**, 2.8 g, 4.8 mmol), bromomethyl anthraquinone (2.71 g, 9.0 mmol), and CsF (1.8 g, 11.8 mmol) were placed in a 250 mL round-bottom flask containing anhydrous DMF (50 mL). The mixture was stirred for 48 h at room temperature. Ethyl acetate (200 mL) was added to the reaction and the mixture washed with water (2 × 50 mL) and dried over Na_2SO_4. The solution was concentrated to a minimum volume until a precipitate formed. The precipitate was filtered, and the filtrate (majority 3′-isomer) was further concentrated and applied to a silica gel column (4.5 × 30 cm) and eluted with CH_2Cl_2/MeOH = 20:1. The desired product (**3**), R_f 0.35, and 3′-isomer (**4**), R_f 0.40, were collected without separation: 1.36 g (50%). ^{1}H NMR (DMSO-d_6) δ 3.50−3.80 (m, 2H, $H_{2'}$ and $H_{3'}$), 4.00, 4.08, 4.15, 4.25 and 4.40 (m, 3H, $H_{4'}$ and $H_{5'}$), 4.70−5.00 (m, 2H, CH_2), 5.30 and 5.45 (m, 2H, $C_{2'}$-OH, $C_{3'}$-OH and $C_{5'}$-OH), 5.75−6.00 (m, 2H, uracil H_5 and $H_{1'}$), 7.50−8.30 (m, 8H, AQ and uracil H_6).

DMT-BzU(2′-UAQ) (5). The two isomers (**3**,**4**, 1.04 g, 1.8 mmol) and DMT-Cl (0.74 g, 2.2 mmol) were dissolved in dry pyridine (20 mL) at room temperature. Concentrated ammonium hydroxide (5 mL) was added to the solution and the solution stirred for 16 h. The mixture was concentrated to dryness under reduced pressure and dissolved in the minimal volume of CH_2Cl_2 and applied to a silica gel column (3 × 45 cm). Elution with CH_2Cl_2/MeOH (20:1) gave two major fractions which were separated as 5′-DMT-U(2′-AQ) (**5**, 905 mg, 1.01 mmol) and 5′-DMT-U(3′-AQ) (**6**, 592 mg, 0.68 mg). Total yield 1.50 g, 95%. **5**: mp 139 °C; TLC (CH_2Cl_2/MeOH = 9:1) R_f 0.67; ^{1}H NMR (DMSO-d_6) δ 3.30 (m, 2 H, $H_{5'}$), 3.72 (s, 6 H, CH_3O of DMT), 4.10(m, 2 H, $H_{2'}$ and $H_{3'}$) 4.28 (ddd, 1 H, becoming dd with D_2O, $H_{3'}$), 4.92 (dd, 2 H, $ArCH_2$), 5.24 (d, 1 H, uracil H_5), 5.47 (d, 1 H, diminished with D_2O 3-OH), 5.95 (d, 1 H, H_1), 6.87 and 7.27 (m, 13 H, DMT), 7.68 (d, 1 H, uracil H_6), 7.90 and 8.20 (m, 7H, AQ), 12.40 (s, 1 H, amide). **6**: mp 141 °C; TLC (CH_2Cl_2/MeOH = 20:1) R_f 0.55; ^{1}H NMR (DMSO-d_6) δ 3.27 (m, 2 H, $H_{5'}$), 3.68 (s, 6H, CH_3O of DMT), 4.13 (m, 2 H, $H_{3'}$ and $H_{4'}$), 4.40 (ddd, 1 H, becoming dd with D_2O, $H_{2'}$), 4.82 (dd, $ArCH_2$), 5.30 (d, 1 H, uracil H_5), 5.72 (d, 1 H, diminished with D_2O, $H_{2'}$) 5.78 (d, 1 H, $H_{1'}$), 6.85 and 7.25 (m, 13 H, DMT), 7.75 (d, 1 H, uracil $H_{6'}$), 7.85 and 8.20 (m, 7 H, AQ).

UAQ Phosphoramidite (7). DMT-Bz(2′-UAQ) (**5**, 234 mg, 0.27 mmol) was dissolved in dry CH_2Cl_2 (3 mL), followed by addition of DIEA (0.24 mL, 1.37 mmol). The mixture was stirred under N_2 until everything dissolved. To this solution, 2-cyanoethyldiisopropylchlorophosphoramidite (0.12 mL, 0.60 mmol) was added dropwise, and the reaction mixture was stirred at room temperature for an additional 30 min and then applied directly to a silica gel column. Elution with CH_2Cl_2/EtOAc/Et_3N (45:45:10) gave one major fraction with R_f 0.65. The solvent was removed under reduced pressure to give pale yellow oil, which was used directly in the DNA synthesis.

Anthraquinone-Oligonucleotide Conjugate Synthesis. The first part of **UAQ-DNA** (before AQ incorporation) was performed on solid phase synthesis following standard conditions, using cyanophophoramidite monomers. When the sample was at the position to couple the AQ monomer, the resin was thoroughly washed and the cartridge (containing the resin) was removed from the synthesizer. The AQ-phosphoramidite monomer was dissolved in 500 μL of a dry CH_3CN solution containing 0.1 M tetrazole. The monomer was taken into the cartridge via a syringe, and the coupling reaction was allowed to proceed

for 20 min, and the monomer solution was removed from the cartridge by pressure injection. The cartridge was placed back onto the synthesizer and the automated sequence was allowed to resume. The coupling efficiency was quantified by measuring the UV-absorption of the trityl cation released and comparing it to that of the previous and subsequent step.

Removal of the oligo from the solid support and subsequent purification by reverse phase HPLC proceeded as usual.

Thermal Denaturation. Samples consisting of equimolar concentrations of DNA oligomers (2.0 μM each) in 1 mL of 10 mM sodium phosphate buffer (pH 7.0) were placed in cuvettes (1.5 mL capacity, 1.0 cm path length) and sealed with tape to prevent evaporation of water during heating/cooling cycles. The absorbance of the samples at 260 nm was monitored as a function of temperature for three consecutive runs: heating 1.0 °C/min and then cooling followed by reheating at 0.5 °C/min. For experiments in which the absorbance was monitored at 330 nm, 20 μM of each oligomer was used due to the low extinction coefficient of AQ chromophore.

The absorbance at 260 nm was plotted against temperature for each sample. Melting temperatures (T_m) were determined as the maxima of the first derivative plot of absorbance versus temperature, assuming a first-order phase transition. The T_m values are given in the tables for all oligomers studied with error values of $\pm$0.5 °C.

Phosphorescence Quenching. Samples were prepared containing 10 μM of oligomer each dissolved in 30% ethylene glycol/sodium phosphate (10 mM, pH 7.0) buffer. Approximately 500 μL of the sample was placed into a standard NMR tube which was then submerged into a liquid nitrogen Dewar flask with quartz windows situated in the sample compartment of a fluorescence spectrometer. Phosphorescence emission spectra from the frozen glass samples were recorded over the range 400−600 nm using the front-face detection mode with excitation at 330 nm. A blank sample containing only the ethylene glycol/sodium phosphate buffer was used to record the baseline.

Cleavage Analysis by Radiolabeling and PAGE. DNA oligonucleotides were radiolabeled either at the 5′- or 3′-end. 5′-OH labeling involved the use of [γ-^{32}P]ATP and bacterial T4 polynucleotide kinase, while 3′-OH labeling involved the use of [α-^{32}P]ddATP and terminal deoxynucleotidyl transferase (TdT). The labeling was performed according to standard procedures. Radiolabeled DNA was purified by 20% PAGE. Samples for irradiation were prepared by hybridizing a mixture of "cold" and radiolabeled oligonucleotide (5 μM) to a total volume of 10 μL each in 10 mM sodium phosphate, pH = 7.0. Hybridization was achieved by heating the samples at 90 °C for 5 min, followed by slow cooling to room temperature over the course of 5 h. Samples were irradiated in microcentrifuge tubes in a Rayonet photoreactor equipped with 8 × 350 nm lamps. After irradiation, the samples were precipitated once with cold ethanol in the presence of glycogen, dried, and treated with 1 M piperidine at 90 °C for 30 min (samples containing 8-OxoG were only treated for 10 min). After evaporation of the piperidine, the samples were dried and suspended in denaturing loading buffer, samples (1500 cpm) were electrophoresed on a 20% 19:1 acrylamide/bis-acrylamide gel containing 7 M urea. The gels were dried, and the cleavage sites were visualized by autoradiography and quantified with a β counter.

Acknowledgment. This work was supported by the National Science Foundation and by the National Institute of Health, for which were are grateful.

Supporting Information Available: Autoradiograms for **UAQ-DNA** with **DNA(1−4)** labeled at the 5′-end and with **UAQ-DNA** labeled at the 3′-end with ^{32}P (PDF). This material is available free of charge via the Internet at http://pubs.acs.org.

JA991753S